Available online at www.sciencedirect.com

ScienceDirect

Physics Procedia 3 (2010) 515–521

Physics Procedia

www.elsevier.com/locate/procedia

International Congress on Ultrasonics, Universidad de Santiago de Chile, January 2009

Ultrasonic field generated by a transducer non axially located at the end of a cylindrical waveguide surrounded by an elastic medium

Slah Yaacoubi[a,c,d], Éric Ducasse[b,c,d]*, Marc Deschamps[c,d], Laurent Laguerre[a]

[a] Laboratoire Central des Ponts et Chaussées, Division Reconnaissance et Mécanique des Sols, Route de Pornic, *BP4129, F-44341, Bouguenais Cedex, France*

[b] *Arts et Métiers Paris Tech, Esplanade des Arts et Métiers, F-33405, Talence, France*

[c] *Université de Bordeaux, UMR5469, 351 cours de la Libération, F-33405, Talence, France*

[d] *CNRS ; UMR 5469, 351 cours de la Libération, F-33405, Talence, France*

Abstract

The calculation of the ultrasonic field generated by a transducer non axially located at the end of a semi-infinite cylindrical waveguide surrounded by an elastic medium is performed. Numerical results representing power flow, waveforms and dispersion diagrams to highlight non-axisymmetric waves are discussed.

Keywords: Dispersion diagrams; displacement waveforms; non-axisymmetric waves; Tensor Hankel transform

1. Introduction

Theoretical studies of guided waves in free elastic bars have been carried out for over one century, since the works of Pochhammer [1] and Chree [2]. Further understanding of the mode propagation solution of Pochhammer has come through the work of Hudson [3] and others. The next major achievements were made numerically by Pao and Mindlin [4] and Zemanek [5] who studied the elastic wave dispersion in 3D free bars. In 1978, Thurston [6] extends these modal solution methods to the leaky case of embedded bars. This numerical study was improved by Pavlacovic in 2001. The case of cylinders including excitation has been studied too. At first, a trapezoidal transient impulse has been studied by Davies [7]. Recently, Puckett and Peterson [8] study the propagation and the reception of ultrasonic displacement field in finite free bars by using normal mode expansion. Laguerre et al. [9] present an alternative semi-analytical formulation based on the integral transform method and Debye series (multiple reflection/refraction acoustic rays).

As an application field, elastic solid bars are used to strengthen structures in many domains like civil and geo-technical engineering [10]-[11]. Unfortunately, defects in these bars could appear due to the mechanical fatigue and

* Corresponding author. Tel.: 33(0)540006222; fax: 33(0)540006964.
E-mail address: e.ducasse@lmp.u-bordeaux1.fr

doi:10.1016/j.phpro.2010.01.067

corrosion [12], rendering their regular inspection as crucial safety insurance. Therefore, techniques based on ultrasonic guided waves, promising means of inspection, attract considerable attention. The waves can be attenuated by the leaks through the sidewalls. In this case, test sensitivity and distance of propagation could be significantly reduced. In non-destructive testing (NDT), dispersion diagrams (i.e representing displacement amplitude versus frequency and wavenumber) play an important role in the study of the influence of the leakage. Classically, these diagrams are calculated by 2D Fourier Transform of waveforms obtained at different positions along the propagation direction in the waveguide [9], [13]. This is computationally inefficient (the time-discretization step must be sufficiently small in order to guarantee the precision of the results).

In this context, on the basis of the tensor Hankel transform (THT), detailed in the related paper [14], we revisit the problem of non-axisymmetric source radiating in an embedded bar. Doing this, the reflected and transmitted field in and out the embedded bar are calculated in the natural 2D spectrum of the guide (k_z, ω). By this way, dispersion diagrams are directly evaluated.

2. Theoretical calculation

2.1. Problem description

A semi-infinite elastic solid bar of radius b is surrounded by an elastic laterally unbounded solid medium, as shown in Fig.1. A source is located at the free section $(z = 0)$ of the waveguide. We assume that its distribution is axisymmetric in its own polar coordinate (r_1, θ_1) and it is delocalized from the center of the free section by (r_0, θ_0). This source, given by its displacement field $\mathbf{u}_{sour}(r, \theta, t)$, is non-axisymmetric in the natural coordinates of the waveguide (r, θ).

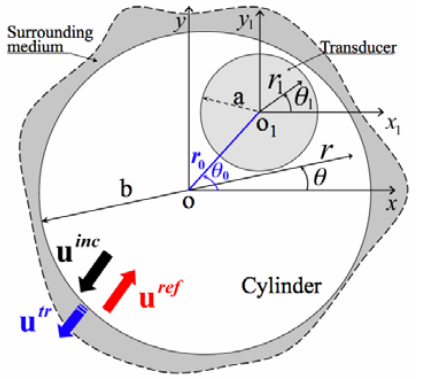

Fig.1 Geometry of the problem: free section $(z = 0)$

The incident displacement field, generated by this source, is noted $\mathbf{u}^{inc}(r, \theta, z, t)$. The reflected field in the waveguide and that transmitted in the surrounding medium are denoted $\mathbf{u}^{ref}(r, \theta, z, t)$ and $\mathbf{u}^{tr}(r, \theta, z, t)$ respectively.

Following the method given in ref [14], any vector field is written as an azimuthal Fourier series expansion:

$$\mathbf{u}(r,\theta,z,t) = \mathbf{u}_0(r,z,t) + \sum_{n=1}^{+\infty} \left[\mathbf{u}_n^{\succ}(r,z,t) \begin{pmatrix} \cos n\theta \\ \sin n\theta \\ \cos n\theta \end{pmatrix} + \mathbf{u}_n^{\perp}(r,z,t) \begin{pmatrix} \sin n\theta \\ -\cos n\theta \\ \sin n\theta \end{pmatrix} \right] \quad (1)$$

For simplicity, since the calculations will be done for a single component $\mathbf{u}_n(r,z,t)$ ($\mathbf{u}_n^{\perp}$ and $\mathbf{u}_n^{\succ}$ are the Fourier coefficients), the indexes $\perp$ and $\succ$ will be omitted henceforth.

2.2. Incident field

It is shown in ref (14), that any field can be expressed in cylindrical coordinates by a time Fourier transform associated with the tensor Hankel transform of first order. The incident field can be then given by:

$$\mathbf{u}_{n,inc}(r,z,t) = \tfrac{1}{2\pi}\int_{-\infty}^{+\infty} e^{i\omega t}\int_{0}^{+\infty} \mathbb{J}_n(k\,r)\,\mathbf{U}_{n,inc}(k,z,\omega)\,k\,dk\,d\omega, \qquad (2)$$

where $\mathbf{U}_{n,inc}(k,z,\omega)$ stands for the spectrum in the (k,z,ω) domain and where k is the radial wavenumber. The kernel of the tensor Hankel transform $\mathbb{J}_n(kr)$ is

$$\mathbb{J}_n = \begin{pmatrix} \frac{1}{2}\left[J_{n-1}+J_{n+1}\right] & \frac{1}{2}\left[-J_{n-1}+J_{n+1}\right] & 0 \\ \frac{1}{2}\left[-J_{n-1}+J_{n+1}\right] & \frac{1}{2}\left[J_{n-1}+J_{n+1}\right] & 0 \\ 0 & 0 & J_n \end{pmatrix}$$

Assuming causality and expanding the incident field into the longitudinal and the transversal waves, the spectrum takes the form:

$$\mathbf{U}_{n,inc}(k,z,\omega) = h(z)\sum_{m=L,T}\mathbf{U}_{n,m}(k,\omega)\,e^{-ik_{z,m}z} \qquad (3)$$

where h is the unit Heaviside function. The terms $\mathbf{U}_{n,m}(k,\omega)$ are deduced after transformation from the field of the source $\mathbf{u}_{sour}(r,\theta,t)$. The variables $k_{z,L}=\sqrt{\omega^2/c_L^2-k^2}$ and $k_{z,T}=\sqrt{\omega^2/c_T^2-k^2}$ are respectively the wavenumbers associated with the longitudinal and the transversal waves.

Applying the Fourier transform in terms of k_z on the frequency spectrum defined by (2), the incident field can be expressed in the (r,k_z,ω) domain by the double integration as follows:

$$\mathbf{U}_{n,inc}(r,k_z,\omega) = \int_{-\infty}^{+\infty}\left[\int_{0}^{+\infty}\mathbb{J}_n(kr)\mathbf{U}_{n,inc}(k,z,\omega)\,k dk\right]e^{ik_z z}dz. \qquad (4)$$

Introducing (3) in (4), swapping the integrals, expanding the integral over k into two parts ($[0,k_c]\cup\,]k_c,+\infty[$) and changing of variables, lead to the below displacement field:

$$\mathbf{U}_{n,inc}(r,k_z,\omega) = \sum_{m=L,T}\left(\mathrm{H}*\mathbf{g}_m\right)(k_z) + \int_{k_{c,m}}^{+\infty}\frac{\mathbf{g}(k)}{i\left(k_{z,m}-k_z\right)}k dk \qquad (5)$$

where $k_{c,m}$ is the cut-off wavenumber and H the Fourier transform of the Heaviside function, which is expressed by:

$$\mathrm{H}(\xi) = \pi\delta(\xi) + \frac{i}{\xi}$$

The function $\mathbf{g}_m$ is given by:

$$\mathbf{g}_m(\xi) = \xi\left[h(\xi)-h\left(\xi-k_{c,m}\right)\right]\mathbf{g}\left(\sqrt{k_{c,m}^2-\xi^2}\right)$$

with

$$\mathbf{g}(\xi) = \mathbb{J}_n(\xi r)\,\mathbf{U}_{n,m}(\xi)\cdot$$

It is of interest to note that the term without integration in (5) describes the travelling waves, while the second term corresponds to the evanescent waves. Far from the source, i. e. for larges values of z, the contribution of

evanescent waves can be neglected. As a consequence, taking into account on the Heaviside function behaviour, the spectrum of the incident field $\mathbf{U}_{n,inc}(r,k_z,\omega)$ can be obtained analytically from (5).

In the next sections, the dependence on n, k_z and ω is implicit. They will be reintroduced only when it is necessary. The function $\mathbf{U}_{n,inc}(r,k_z,\omega)$ can be also obtained in the natural reference of the waveguide, which is defined in [14] by the longitudinal (P), horizontal shear (SH) and vertical shear (SV) cylindrical waves. In such a reference, it is given by

$$\mathbf{U}_{inc} = \mathbb{G}_{out}\mathbf{A}_{inc} \tag{6}$$

where $\mathbf{A}_{inc} = \left(a_{inc,P}\ a_{inc,SH}\ a_{inc,SV}\right)^{\mathrm{T}}$, with T denotes the vector transpose and $a_{inc,P}$, $a_{inc,SH}$ and $a_{inc,SV}$, the amplitudes of the (P, SH, SV) waves. The matrix $\mathbb{G}_{out}(r)$ can be deduced from the matrix $\mathbb{G}$ which is expressed as follows:

$$\begin{bmatrix} \frac{1}{2}\left(-\ell^L_{n-1}+\ell^L_{n+1}\right) & \frac{1}{2}\left(-\ell^T_{n-1}+\ell^T_{n+1}\right) & \frac{1}{2}\left(\ell^T_{n-1}+\ell^T_{n+1}\right) \\ \frac{1}{2}\left(\ell^L_{n-1}+\ell^L_{n+1}\right) & \frac{1}{2}\left(\ell^T_{n-1}+\ell^T_{n+1}\right) & \frac{1}{2}\left(-\ell^T_{n-1}+\ell^T_{n+1}\right) \\ \frac{ik_z}{k_L}\ell^L_n & \frac{-ik_z}{k_L}\ell^T_n & 0 \end{bmatrix} \tag{7}$$

by setting $\ell^m_n = H^{(2)}_n\left(k_m r\right)$. The function $H^{(2)}_n$ denotes the Hankel function of second kind, which describes the outgoing wave in the waveguide. From a numerical point of view, the value of the vector $\mathbf{A}_{inc}$ is obtained by identification with the expression given by (5).

In order to evaluate the reflection coefficients in the waveguide/surrounding interface, let us examine first the radial stress vector $\mathbf{\Sigma}_{inc}$. According to (6), it can be expressed as follows:

$$\mathbf{\Sigma}_{inc}(r) = \mathbb{H}_{out}(r)\,\mathbf{A}_{inc} \tag{8}$$

the matrix $\mathbb{H}_{out}(r)$ is deduced from $\mathbb{H}$, by setting $\ell^m_n = H^{(2)}_n\left(k_m r\right)$ in the following expression:

$$\mathbb{H} = \begin{bmatrix} h_{11} & -k_T\frac{\ell^T_{n-2}-2\ell^T_n+\ell^T_{n+2}}{2} & k_T\frac{\ell^T_{n-2}-\ell^T_{n+2}}{2} \\ k_L\frac{\ell^L_{n-2}-\ell^L_{n+2}}{2} & k_T\frac{\ell^T_{n-2}-\ell^T_{n+2}}{2} & -k_T\frac{\ell^T_{n-2}+\ell^T_{n+2}}{2} \\ 2ik_z\frac{\ell^L_{n-1}-\ell^L_{n+1}}{2} & i\frac{k_z^2-k_T^2}{k_z}\frac{\ell^T_{n-2}-\ell^T_{n+2}}{2} & -ik_z\frac{\ell^T_{n-1}+\ell^T_{n+1}}{2} \end{bmatrix} \tag{9}$$

where $h_{11} = -k_L\left(\frac{\ell^L_{n-2}+\ell^L_{n+2}}{2}+\left(1+\frac{k_z^2-k_T^2}{k_L^2}\right)\ell^L_n\right)$.

The displacement and the radial stress vectors are related by the impedance matrix such that:

$$\mathbf{\Sigma}_{inc}(r) = \mathbb{Z}_{out}(r)\,\mathbf{U}_{inc}(r), \tag{10}$$

where: $\mathbb{Z}_{out}(r) = \mathbb{H}_{out}(r)\left[\mathbb{G}_{out}(r)\right]^{-1}$.

2.3. Reflected and transmitted fields

Referring to (6), the reflected field in the (r,k_z,ω) domain can be written as follows:

$$\mathbf{U}_{ref}(r) = \mathbb{G}_{in}(r)\,\mathbf{A}_{ref} \tag{11}$$

where $\mathbb{G}_{in}(r)$ is deduced from the matrix $\mathbb{G}$ given by (7) setting $\ell_n^m = J_n(k_m r)$ with J_n the Bessel function of first kind, which identify the ingoing waves. The reflected radial stress vector $\mathbf{\Sigma}_{ref}$ is then:

$$\mathbf{\Sigma}_{ref}(r) = \mathbb{H}_{in}(r)\,\mathbf{A}_{ref} \tag{12}$$

and the impedance matrix has the form:

$$\mathbb{Z}_{in}(r) = \mathbb{H}_{in}(r)\left[\mathbb{G}_{in}(r)\right]^{-1}$$

here $\mathbb{H}_{in}(r)$ is deduced from the matrix $\mathbb{H}$ (see (9)) with $\ell_n^m = J_n(k_m r)$. According to (6) and (11), the transmitted field in the (r, k_z, ω) domain is given by:

$$\mathbf{U}_{tr}(r) = \mathbb{G}^{\bullet}_{out}(r)\,\mathbf{A}_{tr} \tag{13}$$

where $\mathbb{G}^{\bullet}_{out}(r)$ is obtained from the matrix $\mathbb{G}$ (7) by setting $\ell_n^m = H_n^{(2)}\left(k_m^{\bullet} r\right)$. The wavenumbers $k_m^{\bullet}$ refer in this case to the surrounding medium. The transmitted radial stress $\mathbf{\Sigma}_{tr}$ vector takes the form:

$$\mathbf{\Sigma}_{tr}(r) = \mathbb{H}^{\bullet}_{out}(r)\,\mathbf{A}_{tr} \tag{14}$$

and the impedance matrix is expressed by:

$$\mathbb{Z}^{\bullet}_{out}(r) = \mathbb{H}^{\bullet}_{out}(r)\left[\mathbb{G}^{\bullet}_{out}(r)\right]^{-1}$$

$\mathbb{H}^{\bullet}_{out}(r)$ is deduced from the matrix $\mathbb{H}$, cf. the matrix (9) with $\ell_n^m = H_n^{(2)}\left(k_m^{\bullet} r\right)$. The continuity conditions of displacement and normal stress vectors leads to the 3x3 reflection matrix:

$$\mathbf{A}_{ref} = \mathbb{R}(b)\,\mathbf{A}_{inc}\,, \tag{15}$$

where $\mathbb{R}(b) = -\mathbb{G}_{in}^{-1}(b)\,\mathbb{Z}(b)\left[\mathbb{Z}^{\bullet}_{out}(b) - \mathbb{Z}_{out}(b)\right]\mathbb{G}_{out}(b)$ and $\mathbb{Z}(b) = \left[\mathbb{Z}^{\bullet}_{out}(b) - \mathbb{Z}_{in}(b)\right]^{-1}$. The transmission matrix has the form

$$\mathbf{A}_{tr} = \mathbb{T}(b)\,\mathbf{A}_{inc}$$

where $\mathbb{T}(b) = \mathbb{G}_{out}^{-1}(b)\,\mathbb{Z}(b)\left[\mathbb{Z}_{out}(b) - \mathbb{Z}_{in}(b)\right]\mathbb{G}_{out}(b)$. The subscript $(\bullet)$ indicates the outgoing waves in the surrounding medium.

Finally, the partial reflected and transmitted fields in the space-time domain are given respectively by:

$$\mathbf{u}_{n,ref}(r,z,t) = \int_{-\infty}^{+\infty}\int_{-\infty}^{+\infty} \mathbb{G}_{in}(r,k_z,\omega)\,\mathbf{A}_{ref}(k_z,\omega)\,e^{i(\omega t - k_z z)}\,dk_z\,d\omega \tag{16}$$

$$\mathbf{u}_{n,tr}(r,z,t) = \int_{-\infty}^{+\infty}\int_{-\infty}^{+\infty} \mathbb{G}^{\bullet}_{out}(r,k_z,\omega)\,\mathbf{A}_{tr}(k_z,\omega)\,e^{i(\omega t - k_z z)}\,dk_z\,d\omega\,. \tag{17}$$

Both total reflected and transmitted fields can be then calculated by injecting (16) and (17) respectively in (1).

3. Numerical simulations and discussions

Numerical simulations are performed for a circular cylindrical steel bar surrounded by a cement grout. The excitation produced by the transducer is a combination of Gaussian beam and time Gaussian pulse. This excitation is given in the coordinate source (r_1, θ_1) (see Fig.1) by:

$$\mathbf{u}(r_1)_{sour} = \left(0 \quad 0 \quad u_0\, \mathrm{e}^{-\pi r_1^2 \alpha^{-2}}\right)^{\mathrm{T}} e(t),\ r_1 < \mathrm{a}\,. \tag{18}$$

where a is the radius of the source.

By mean of the addition theorem [15], this displacement field can be expressed in the (r,θ) coordinates of the waveguide. By using the THT, we obtain after some algebra,:

$$\sum_{m=L,T} \mathbf{U}_{n,m}(k,\omega) = \left(0 \;\; 0 \;\; u_0 \, e^{-\alpha^2 k^2/4\pi}\right)^{\mathrm{T}} e^{-in\theta_0} \, \mathbb{J}_n(kr_0) \qquad (19)$$

For numerical applications, we take $u_0 = 1$, $\alpha = 2\ mm$, $\theta = \theta_0 = 0$, $r = 8\ mm$, $c_L = 5960$ and $c_T = 3260$ for cement, $c_L = 2810$ and $c_T = 1700\ ms^{-1}$ for steel.

In order to study the non-axisymmetric waves, the influence of the off-axis distance of the source on the displacement waveforms is studied for various distances from the source. When the source is located off the cylinder axis, the higher circumferential modes (n>0) enter into the description of the source, which is therefore more complicated. When the source is on the cylinder axis, only the mode (n=0) contributes to the solution. Comparison of these two cases is shown in Fig.2. We display some normalized displacement waveforms at the axial distances $z = 100,\ 200$ and $300\ mm$; the source is firstly located on the cylinder axis $r_0 = 0$ (left), moved then to $r_0 = 2\ mm$ (middle). The differences of their normalized amplitudes are given in the right column. As it can be remarked, the amplitude differences are not slight and signals are shorter when the source is delocalized due to the distance between the source and the detector. This shows that non-axisymmetric waves are important and can not be neglected. These waves should have a great deserve in localization and sizing of defects.

In NDT field, it is useful to express the ultrasonic field under inspection (*e.g.,* displacement, pression…) in the 2D frequency/wavenumber domain. This representation in this domain defines the so-called *dispersion diagram.*

In both numerical and experimental works, this diagram is usually performed by applying a 2D FFT to the matrix constituted by the waveforms obtained for several locations in the propagation direction (see for example [13], [16]). However, as made clear from (11), the function $\mathbf{U}_{ref}(r,k_z,\omega)$ gives directly these diagrams. In this way, from a numerical point of view, a significant saving in computing time is noteworthy.

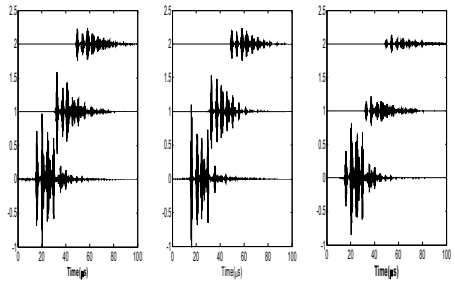

Fig.2 Normalized displacement waveforms for $r_0 = 0$ (left), $r_0 = 2\ mm$ (middle) and their differences (right) at $z = 100,\ 200,\ 300\ mm$ (from the bottom to the top).

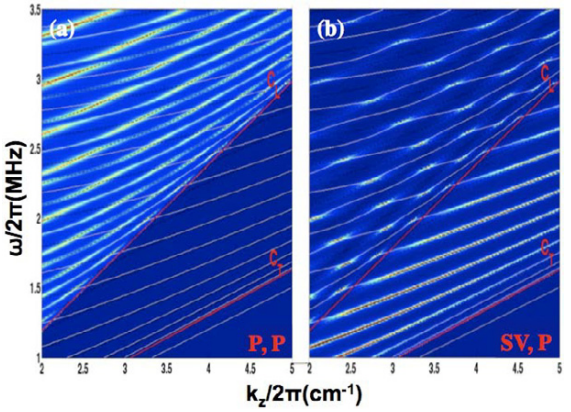

Fig.3 Superposition of displacement dispersion diagrams and dispersion curves (few lines) simulated for $\frac{f}{2\pi} \in [1.5;3.5]\ MHz$ and $\frac{k_z}{2\pi} \in [2;5]\ cm^{-1}$.

An example of the interpretation of such diagrams is illustrated in Fig.3 for the lowest flexional waves (n=*1*) and at the given position $(r = 8\ mm)$, where $\mathbf{U}_{ref}$ maximum amplitude (blue 0, dark white max) coincides with the guided modes solution of generalized Pochhammer equation in a surrounded cylinder. These curves are derived

from Disperse software [17]. On one hand, a good agreement is found between these diagrams and dispersion curves. On the other hand, since the dispersion diagrams depend on the excitation (form and nature), some physical remarks can be extracted, as plan portion limited by C_L and C_T line is created only when the incident and reflected waves are shear, figure (*b*). In addition, when the incident and reflected waves are the same and consequently as which is well known, there is no mode conversion figures (*a*). Whereas, in figure (*b*), mode conversions are clear.

4. Conclusion

A mathematical model has been developed in synthetic form. Numerical simulations have been performed for a Gaussian beam excitation. Special attention is paid to the non-axisymmetric waves through the study of the influence of the off-axis distance of the source on the displacement waveforms for various axial propagation distances. This emphasizes the importance of studying the non-axisymmetric waves. The dispersion diagrams (ω, k_z) have been inspected directly. An excellent agreement between the latter diagrams and dispersion curves is found. The combination of this method and Debye series for well understanding the interaction with the sidewalls will be presented in next work.

References

[1] J. Pochhammer, "Ueber die Fortpflanzungsgeschwindigkeiten kleiner schwingungen in einem unbegrenzten isotropen kreiszylinder," J. fuer reine und angewandte Math, 81, 324-336, 1876.
[2] C. Chree, "The equations of an isotropic elastic solid in polar and cylindrical coordinates, their solutions and applications," Transactions of the Cambridge Philosophical Society, 14, 324-369, 1889.
[3] G. E. Hudson, "Dispersion of elastic waves in solid circular cylinders," Physics Review, 63, 46-51, 1943.
[4] Y.H. Pao and R. Mindlin, "Dispersion of flexural waves in an elastic circular cylinder," J. of App. Mech, 27, 513-520, 1960.
[5] J. Zemanek, "An experimental and theoretical investigation of elastic wave propagation in a cylinder," J. Acoust. Soc. Am, 51, 265-283, 1972.
[6] R. Thurston, "Elastic waves in rods and clad rods," J. Acoust. Soc. Am, 64, 1-35, 1978.
[7] R. M. Davies, "A critical study of the Hopkinson," Ultrasonics, 43, 197-207, (2005).
[8] A. Puckett, and M. Peterson, "A semi-analytical model for predicting multiple waveguide propagating axially symmetric modes in cylindrical waveguides," Ultrasonics, 43, 197-207, (2005).
[9] L. Laguerre, A. Grimault and M. Deschamps, "Ultrasonic transient bounded-beam propagation in solid cylinder waveguide embedded in solid medium," J. Acoust. Soc. Am, 121, 1924-1934, 2007.
[10] A. Azizinamini M. Strak, J. J. Roller and S. K. Ghosh, "Bond performance of reinforcing bars embedded in high-strength concrete," Structural Journal, 90, 554-561, 1993.
[11] M. D Bear and M. Lowe, "Non-destructive testing of rock bolts using guided ultrasonic waves," Int. J. Rock Mech. Min. 40, 527-536, 2003.
[12] J. A. Gonzàlez, C. Andrade, C. Alonso, S. Feliu, "Comparison of rates of general corrosion and maximum pitting penetration on concrete embedded steel reinforcement," 25, 257-264, 1995.
[13] D. Alleyne and P. Cawley, "A two-dimensional Fourier transform method for the measurement of propagating multimode signals," J. Acoust. Soc. Am, 89, 1159-1167, 1991.
[14] É. Ducasse and S. Yaacoubi, "The Hankel transform of first and second-order tensor fields: definition and use for modeling circular symmetric leaky waveguides," ICU 2009, Santiago, Chile.
[15] J. A. Stratton, "Electromagnetic theory," McGraw-Hill, New York and London, 1949.
[16] E. G. Williams, B. H. Houston and J. A. Bucaro, "Experimental investigation of the wave propagation on a point-driven, submerged capped cylinder using K-space analysis," J. Acoust. Soc. Am, 87, 513-522, 1990.
[17] "Disperse software",www.imperial.ac.uk/ndt/public/ product service/Disperse.html